

Characterization of porous carbon nanofibers decorated with Pt catalysts for use as counter electrodes in dye-sensitized solar cells

HyeLan An, Geon-Hyoung An and Hyo-Jin Ahn*

Department of Materials Science and Engineering, Seoul National University of Science and Technology 139-743 Seoul, Korea

Porous carbon nanofibers decorated with Pt catalysts (Pt/PCNFs) are prepared by electrospinning and impregnation methods. To synthesize the PCNF, poly(styrene-co-acrylonitrile) (SAN), a pore-forming agent, is added to polyacrylonitrile (PAN), the carbon nanofiber (CNF) precursor. With regard to photovoltaic properties, Pt/PCNFs fabricated using the optimum amount of 0.5 wt% SAN polymer exhibit a larger open circuit voltage (V_{oc}) of 0.73 V, a higher fill factor (FF) of 66.57%, and an excellent photoconversion efficiency (η) of 6.47% compared to carbon nanofibers decorated with Pt catalysts (Pt/CNFs) and commercial Pt solutions under standard test conditions (100 mW/cm² (1 sun); AM 1.5G spectrum).

Key words: Porous carbon nanofibers, Counter electrode, Electrospinning, Dye-sensitized solar cells.

Introduction

Dye-sensitized solar cells (DSSCs) are of interest due to simple and cost-effective manufacturing process, together with improved possibilities for the fabrication of transparent and flexible devices compared to silicon solar cells [1, 2]. In general, DSSCs are primarily composed of a sensitizer composed of Ru-based dyes, a working electrode based on a semiconductor, electrolytes based on the iodide/triiodide redox couple, and a counter electrode based on catalyst materials. In particular, for a counter electrode, Pt has been used most commonly as a catalyst because of its excellent conductivity and superb catalytic activity, specifically in the reduction of triiodide ions in electrolyte. Despite these advantages, considerable issues such as high price and finite resources currently exist as barriers to industrialization. In this context, various alternatives to Pt catalysts or the reduction of Pt catalysts are essential to achieve cost effective, high-performance DSSCs [2]. To date, alternative materials such as inorganic semiconductors (CoS, NiS, TiN, MoN, Fe₂N), conducting polymers (polypyrrole, polyaniline, poly(3,4-ethylenedioxythiophene)-poly(styrenesulfonate) (PEDOT-PSS)), and carbon-based materials (graphite, carbon nanotubes (CNTs), CNFs) have been investigated [3]. Among these, CNFs were chosen because of advantages such as large surface area (448 m²/g), high electrical conductivity (10⁵ S/cm), excellent electrochemical stability, and superior catalytic performance [4, 5]. Compared to the price of Pt (~ 50 \$/g), the price of CNF (~ 0.3 \$/g) is more economical, and this differential has resulted in increased

interest in CNFs from researchers [6]. For example, Joshi et al. synthesized CNFs with a low charge-transfer resistance and fast redox reaction rate as a counter electrode for DSSCs. These CNFs demonstrated excellent photovoltaic properties with a V_{oc} of 0.76 V, J_{sc} of 12.60 mA/cm², and η of 5.5% [7]. Noh et al. reported that a counter electrode fabricated with CNF composites composed of 40 wt% Pt nanoparticles exhibited a η of 4.47% [8]. A study utilizing porous CNFs with a SAN polymer as a pore-foaming agent and well-dispersed Pt catalysts has not previously been reported in the field of DSSCs. Thus, we synthesized porous CNFs decorated with Pt catalysts and demonstrated their morphological, structural, and electrochemical catalytic activity for use as a counter electrode in DSSCs.

Experiments

Conventional CNFs and PCNFs were synthesized by an electrospinning method. In the case of bare CNFs, poly(vinylpyrrolidone) (PVP, $M_w = 1,300,000$ g/mol, Aldrich) and PAN ($M_w = 150,000$ g/mol, Aldrich) were added into *N,N*-dimethylformamide (DMF, Aldrich) and the mixed solution is stirred for 5 h. To synthesize PCNFs, SAN ($M_w = 165,000$ g/mol, Aldrich) was added to the above mixed solution to obtain improved catalytic properties. During the electrospinning process, the prepared solution was loaded into a syringe, and then the potential and feeding rates were fixed at ~ 13 kV and ~ 0.03 mL/h, respectively. The prepared as-spun nanofibers were stabilized in air at 280 °C for 2 h and then carbonized at 800 °C for 2 h in N₂ atmosphere. Conventional CNFs and PCNFs were treated with an acidic solution consisting of HF and HNO₃ (1 : 1 (v/v)) to enable the formation of functional groups such as -COOH, -OH, and C=O on the CNF surface. As a

*Corresponding author:
Tel : +82-2-970-6622
Fax: +82-2-973-6657
E-mail: hjahn@seoultech.ac.kr

result, the functional groups enable the successful synthesis of Pt catalysts onto the CNF surface during impregnation owing to the increased number of anchoring sites between the metal-ligand systems of Pt catalysts and the formed functional groups [9]. To decorate the conventional CNFs and PCNFs with Pt catalysts, the CNF supports and chloroplatinic acid hydrate ($\text{H}_2\text{PtCl}_6 \cdot 6\text{H}_2\text{O}$, Aldrich) were evenly dispersed in deionized (DI) water. Then, NaBH_4 , a reducing agent, was added to the dispersed solution to facilitate loading of Pt catalysts onto the CNF supports. The resultant samples were washed several times using DI water and then freeze-dried at -50°C . In summary, conventional CNFs, porous CNFs, conventional CNFs decorated with Pt catalysts, and porous CNFs decorated with Pt catalysts were synthesized by using electrospinning and/or impregnation methods (referred to herein as CNFs, PCNFs, Pt/CNFs, and Pt/PCNFs, respectively) for use as counter electrodes in DSSCs. For comparison, a commercial Pt electrode was prepared by spin-coating using a 5 mM solution of $\text{H}_2\text{PtCl}_6 \cdot 6\text{H}_2\text{O}$ in 2-propanol and sintering at 450°C for 0.5 h. A carbon-based counter electrode for DSSCs was prepared using a squeeze-printing method. Paste inks consisting of as-prepared samples, Ketjen black (KJB, Alfa Aesar), and polyvinylidene difluoride (PVDF, Alfa Aesar) at a ratio of 7 : 2 : 1 in N-methyl-2-pyrrolidone (NMP, SAMCHUN) were coated on F-doped SnO_2 (FTO, $8\ \Omega/\text{sq}$, Pilkington) and dried at 100°C for 12 h. A working electrode for DSSCs was prepared by a conventional method as follows. Paste inks containing TiO_2 (P25, Degussa AG), hydroxypropyl cellulose (HPC, Mw $\sim 80,000$ g mol, Aldrich), acetyl acetone (Aldrich), and DI water were coated on the FTO substrate using a squeeze-printing method. Afterward, the electrode was sintered at 500°C for 1 h, followed by soaking in 0.5 mM dye solution comprising N719 dye (Ru-535-bisTBA, Solaronix) to promote dye absorption, and immersion in ethanol for 24 h. Finally, the dye-adsorbed TiO_2 electrode and prepared counter electrode were firmly assembled into sandwich-type cells and the intercellular space was filled with iodide/triiodide-based redox electrolytes consisting of iodine (I_2 , Merck KGaA), 1-butyl-3-methylimidazolium iodide (BMII, Aldrich), guanidine thiocyanate (GuSCN, Aldrich), and 4-tert-butylpyridine (4TBP, Aldrich) in a solution of acetonitrile/valeronitrile (85 : 15 (v/v)).

The morphological and structural properties of the resultant samples were examined by field-emission scanning electron microscopy (FESEM; Hitachi S-4800) and transmission electron microscopy (MULTI/TEM; Tecnaï G², KBSI Gwangju Center). Brunauer-Emmett-Teller measurements (BET; Micromeritics ASAP2010) provided information regarding the specific surface area and total pore volume of the samples. X-ray diffraction (XRD; $\text{Cu K}\alpha$ radiation, Rigaku D/Max 2500V) characterized the crystal structure of the specimen. To analyze the electrical properties of a counter electrode in

DSSCs, electrochemical impedance spectra (EIS) was performed using Potentiostat/Galvanostat (PGST302N, Eco chemie) with an AC signal of 10 mV in a frequency range of 100 kHz to 0.5 Hz. The photovoltaic properties of the DSSC cells were measured using Solar Simulator (PEC L01, 150 Watt Xenon Arc Lamp, Peccell technologies, Japan) under AM 1.5G spectra with an intensity of $100\ \text{mW}/\text{cm}^2$.

Results and Discussion

Fig. 1 shows the SEM images obtained from (a) CNFs, (b) PCNFs, (c) Pt/CNFs, and (d) Pt/PCNFs. Conventional CNFs and PCNFs fabricated by electrospinning exhibited a smooth surface, whereas the Pt/CNFs and Pt/PCNFs exhibited relatively rough surfaces due to the existence of Pt catalysts on the CNF surface. In addition, diameters of the Pt/CNFs ($\sim 228\text{--}248$ nm) and Pt/PCNFs ($\sim 210\text{--}247$ nm) are slightly increased as compared to those of conventional CNFs ($\sim 200\text{--}234$ nm) and PCNFs ($\sim 195\text{--}245$ nm) owing to the Pt catalysts present on the CNF supports. Furthermore, the Pt/PCNFs display a smaller agglomeration of Pt nanoparticles than that of the Pt/CNFs, thereby implying that the Pt nanoparticles on the porous CNFs are well distributed.

Figs. 2(a-d) and 2(e-h) exhibit TEM and enlarged TEM images obtained from CNFs, PCNFs, Pt/CNFs, and Pt/PCNFs. TEM measurements are performed to investigate whether a relationship exists between the morphological properties of the fibers and the dispersion degree of the Pt catalysts and pore structures of the CNFs. For the conventional CNFs and PCNFs, a clear contrast is observed, as shown in Figs. 2(a) and 2(b). That is, conventional CNFs present a uniform dark gray contrast. However, PCNFs possess a relatively bright contrast region in the CNF matrix that implies

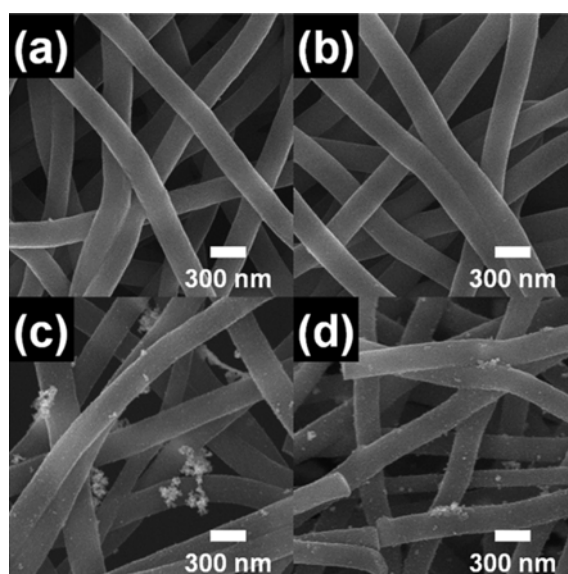


Fig. 1. SEM images obtained from (a) conventional CNFs, (b) PCNFs, (c) Pt/CNFs, and (d) Pt/PCNFs.

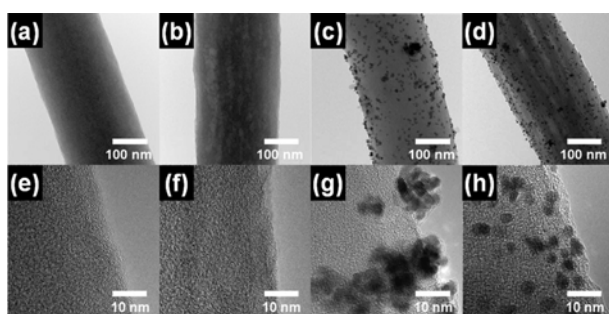


Fig. 2. TEM [(a)–(d)] and enlarged TEM images [(e)–(h)] obtained from conventional CNFs, PCNFs, Pt/CNFs, and Pt/PCNFs.

high porosity of the CNFs. In particular, the formation of PCNFs with a high specific surface area is because of the addition of a SAN polymer (pore-forming agent) into a PAN solution. Specifically, the fibers were decomposed for carbonization, and then pores formed at the sites of SAN burnout [10]. Figs. 2(c) and 2(d) reveal dark splotches indicative of the Pt catalysts present on the conventional CNFs and PCNFs; their diameters are observed to be $\sim 4\text{--}7$ nm. For the Pt/CNFs, a large agglomeration of Pt catalysts on the CNF surface is observed. However, for the Pt/PCNFs, Pt catalysts deposited on the CNF surface are observed to be well-dispersed, as shown in Figs. 2(d) and 2(h). These results indicate that porosity contributes to the improved dispersion of Pt catalysts onto the CNF surface and to the achievement of high catalytic characteristic in DSSCs.

The specific surface area and total pore volume for the PCNFs were analyzed using BET measurement. To investigate the optimum condition of the SAN polymer as a pore-forming agent, we tested three different amounts of SAN, 0.2, 0.5, and 1 wt%, which correspond to higher specific surface areas of ~ 953 , ~ 1136 , and ~ 923 m^2/g and larger total pore volume of ~ 0.494 , ~ 0.549 , and ~ 0.477 cm^3/g , respectively, compared to the conventional CNFs of ~ 463 m^2/g and 0.219 cm^3/g . In particular, the PCNFs with 0.5 wt% SAN display not only the highest specific surface area but also the largest pore volume among the samples. These properties of the PCNFs provide more many active sites to facilitate the improved dispersion of Pt catalysts onto the CNF surface, rapid penetration of the electrolyte, and increased contact area between the Pt catalysts and the electrolyte [11]. Therefore, the PCNFs with the optimum amount of SAN, 0.5 wt%, were adopted as catalyst supports for high-performance counter electrode in DSSCs.

Fig. 3 shows the XRD patterns of conventional CNFs, PCNFs, Pt/CNFs, and Pt/PCNFs. For the conventional CNFs and PCNFs, two broad peaks are present at $\sim 25^\circ$ and 43° , corresponding to the (002) and (100) planes of graphite, respectively. The Pt/CNFs and Pt/PCNFs have observed characteristic diffraction peaks at $2\theta = 39.7^\circ$, 46.2° , 67.3° , and 81.3° , corresponding to

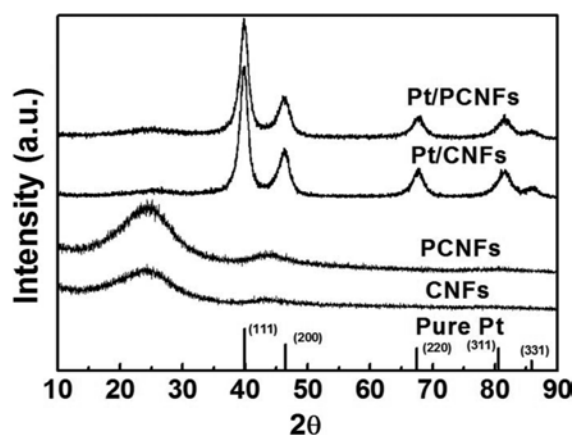


Fig. 3. XRD patterns obtained from conventional CNFs, PCNFs, Pt/CNFs, and Pt/PCNFs. The reference line of pure Pt phases is shown in the bottom (JCPDS card No. 04-0802).

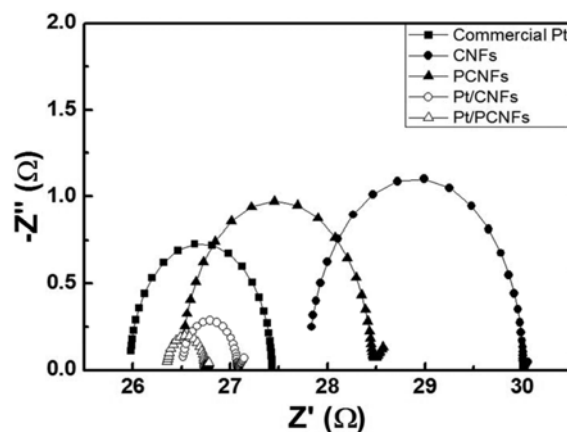


Fig. 4. Nyquist plot of symmetrical cells obtained from the commercial Pt, conventional CNFs, PCNFs, Pt/CNFs, and Pt/PCNFs.

(111), (200), (220), and (311) planes, that are identified as face-centered cubic Pt phase (JCPDS card No. 040802, space group $Fm\bar{3}m[225]$). Furthermore, the grain size of Pt nanoparticles present on the CNFs can be calculated according to the Scherrer equation by using the (111), (200), (220), and (311) planes as below:

$$D = 0.9\lambda/\beta\cos\theta \quad (1)$$

where D , λ , β , and θ are the average size of nano-sized particles, wavelength of X-ray radiation, intensity of full width at half maximum (FWHM), and Bragg's angle, respectively. The average grain sizes are ~ 5.0 nm for Pt/CNFs and ~ 4.8 nm for Pt/PCNFs, which was in good agreement with TEM results.

Impedance measurements were carried out to obtain the information on the performances of the electrodes, as shown in Fig. 4. Electrochemical impedance spectroscopy (EIS) was performed by using symmetrical cells fabricated with two identical electrodes containing the commercial Pt, conventional CNFs, PCNFs, Pt/CNFs, and Pt/PCNFs, which were measured in a frequency

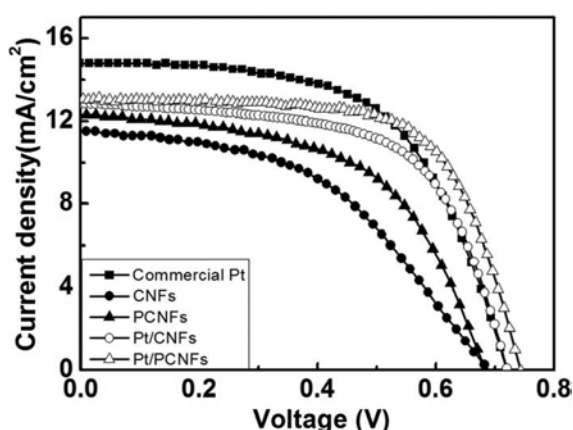


Fig. 5. Photoconversion efficiency from solar energy to electricity obtained from DSSCs fabricated with the commercial Pt electrode, conventional CNFs, PCNFs, Pt/CNFs, and Pt/PCNFs through solar simulator.

Table 1. Parameter summary of photovoltaic performance for the Pt solution, conventional CNFs, PCNFs, Pt/CNFs, and Pt/PCNFs as counter electrode.

Samples	V _{oc} (V)	J _{sc} (mA/cm ²)	FF (%)	PCE (%)
Commercial Pt	0.72 ± 0.1	14.79 ± 0.2	58.9 ± 0.2	6.27 ± 0.1
Conventional CNFs	0.68 ± 0.1	11.57 ± 0.2	46.76 ± 0.1	3.73 ± 0.1
PCNFs	0.68 ± 0.1	12.32 ± 0.2	55.02 ± 0.2	4.63 ± 0.2
Pt/CNFs	0.73 ± 0.1	12.85 ± 0.2	61.68 ± 0.2	5.71 ± 0.1
Pt/PCNFs	0.73 ± 0.1	13.09 ± 0.2	66.57 ± 0.1	6.47 ± 0.2

range of 100 kHz to 0.5 Hz at an AC signal of 10 mV. Nyquist plot in EIS exhibits the series resistance (R_s) at high-frequency region and semicircle relative to charge-transfer resistance (R_{ct}), which is mainly used to examine the electrocatalytic activity of a counter electrode in DSSCs. The R_{ct} values of the samples are $\sim 1.46 \Omega$ for commercial Pt, $\sim 2.21 \Omega$ for conventional CNFs, $\sim 1.94 \Omega$ for PCNFs, $\sim 0.56 \Omega$ for Pt/CNFs, and $\sim 0.39 \Omega$ for Pt/PCNFs, respectively. In other words, these results indicate that Pt/PCNFs shows the lowest R_{ct} value among the other samples owing to increase of the contact area between the Pt catalysts and the electrolyte resulting in the well-dispersed Pt catalysts on PCNFs [12].

Fig. 5 displays the photocurrent density-voltage (J-V) curves used to examine the η of the commercial Pt, conventional CNFs, PCNFs, Pt/CNFs, and Pt/PCNFs as counter electrodes in DSSCs. Their photovoltaic performance is summarized in Table 1. The conversion efficiency of DSSCs is calculated according to the equation below:

$$\eta(\%) = (J_{sc} \times V_{oc} \times FF) / P_{in} \quad (2)$$

where η , J_{sc} , V_{oc} , FF, and P_{in} are the photoconversion efficiency, short circuit current density, open circuit

voltage, fill factor, and intensity of the incident light (100 mW/cm²), respectively. The DSSCs fabricated with commercial Pt electrode exhibited an V_{oc} of ~ 0.72 V, a J_{sc} of ~ 14.79 mA/cm², and a FF of $\sim 58.90\%$, leading to η of $\sim 6.27\%$. The η of DSSCs fabricated with the prepared samples is $\sim 3.73\%$ for conventional CNFs, $\sim 4.63\%$ for PCNFs, $\sim 5.71\%$ for Pt/CNFs, and $\sim 6.47\%$ for Pt/PCNFs, respectively. Though DSSCs fabricated with the CNFs exhibited much lower efficiencies compared to DSSCs fabricated with a commercial Pt counter electrode, the CNFs are still considered good supports because of their inherent advantages such as low-cost, chemical stability, high mechanical strength, and good conductivity. Therefore, the Pt/PCNFs exhibit excellent photovoltaic properties compared to other samples. In particular, the Pt/PCNFs present improved a η of $\sim 6.47\%$, including an V_{oc} of ~ 0.73 V, a J_{sc} of ~ 13.09 mA/cm², and a FF of $\sim 66.57\%$, respectively. This performance enhancement is because the PCNFs have a high specific surface area and a large pore volume that allows the Pt catalysts to be well-dispersed, thereby enhancing the electrocatalytic activity of the counter electrode and improving the reduction of triiodide ions in the electrolyte of DSSCs [5, 11]. These results indicate that porous CNFs decorated with well-dispersed Pt catalysts can be used as counter electrodes in DSSCs and that their use could positively impact DSSCs as follows: (1) significantly improve the photovoltaic performance of the cells, and (2) reduce the cost of the Pt associated with the cells due to the low loading of Pt catalysts.

Conclusions

Pt/PCNFs were synthesized using a combination of an electrospinning and an impregnation method. The porous CNFs fabricated using the optimum amount of 0.5 wt% SAN polymer have well-dispersed Pt catalysts compared to the conventional CNFs due to a high surface area (1136 m²/g) and a large pore volume (0.5497 cm³/g). Thus, the Pt/PCNFs exhibited excellent η (6.47%) high J_{sc} (13.09 mA/cm²) and high FF (66.57%), compared to the other samples. The performance enhancement observed in the Pt/PCNFs is because the Pt catalysts are well-dispersed onto the porous CNFs due to an increased contact area between the Pt catalysts and the electrolyte. This phenomenon can affect the high-performance of DSSCs. Thus, the use of Pt/PCNFs as a counter electrode in DSSCs might be a good alternative to traditional Pt catalysts used for high-performance DSSCs.

Acknowledgments

This work was supported by grant No. 10046672 from the Ministry of Knowledge Economy (MKE) and

R&D Program for Technology of Specialized Materials particularly designed for venture business funded by the Ministry of Knowledge, Republic of Korea.

References

1. M. Grätzel, *Nature* 414 (2001) 338-344.
2. J.-Y. Lin, J.-H. Liao, and T.-C. Wei, *Electrochem. Solid-State Lett.* 14 (2011) D41-D44.
3. Y. Hou, D. Wang, X.H. Yang, W.Q. Fang, B. Zhang, H.F. Wang, G.Z. Lu, P. Hu, H.J. Zhao, and H.G. Yang, *Nat. Commun.* 4 (2013) 1583-1590.
4. W. Kwon, J.-M. Kim, and S.-W. Rhee, *J. Mater. Chem. A* 1 (2013) 3202-3215.
5. G.-H. An, and H.-J. Ahn, *Electrochem. Solid State Lett.* 3 (2014) M29-M32.
6. D. Sebastián, V. Baglio, M. Girolamo, R. Moliner, M.J. Lázaro, and A.S. Aricò, *J. Power Sources* 250 (2014) 242-249.
7. P. Joshi, L. Zhang, Q. Chen, D. Galipeau, H. Fong, and Q. Qiao, *Appl. Mater. Interfaces* 2 (2010) 3572-3577.
8. S.I. Noh, T.-Y. Seong, and H.-J. Ahn, *J. Ceram. Process. Res.* 13 (2012) 491-494.
9. T.G. Ros, A.J. Dillen, J.W. Geus, and D.C. Koningsberger, *Chem. Eur. J.* 8 (2002) 1151-1162.
10. B.-S. Lee, S.-B. Son, K.-M. Park, G. Lee, K.H. Oh, S.-H. Lee, and W.-R. Yu, *Appl. Mater. Interfaces* 4 (2012) 6702-6710.
11. T. Peng, W. Sun, X. Sun, N. Huang, Y. Liu, C. Bu, S. Guo, and X.-Z. Zhao, *Nanoscale* 5 (2013) 337-341.
12. F. Gong, H. Wang, and Z.-S. Wang, *Phys. Chem. Chem. Phys.* 13 (2011) 17676-17682.